

Projected Stein Variational Gradient Descent

Peng Chen¹ Omar Ghattas¹

Abstract

The curse of dimensionality is a critical challenge in Bayesian inference for high dimensional parameters. In this work, we address this challenge by developing a *projected Stein variational gradient descent* (pSVGD) method, which projects the parameters into a subspace that is adaptively constructed using the gradient of the log-likelihood, and applies SVGD for the much lower-dimensional coefficients of the projection. We provide an upper bound for the projection error with respect to the posterior and demonstrate the accuracy (compared to SVGD) and scalability of pSVGD with respect to the number of parameters, samples, data points, and processor cores.

1. Introduction

Given observation data for a system with unknown parameters, Bayesian inference provides an optimal probability framework for learning the parameters by updating their prior distribution to a posterior distribution. However, many conventional methods for solving high-dimensional Bayesian inference problems face the curse of dimensionality, i.e., the computational complexity grows rapidly, often exponentially, with respect to (w.r.t.) the number of parameters. To address the curse of dimensionality, the intrinsic properties of the posterior distribution, such as its smoothness, sparsity, and intrinsic low-dimensionality, have been exploited to reduce the parameter correlation and develop efficient methods whose complexity grows slowly or remains the same with increasing dimension. By exploiting the geometry of the log-likelihood function, accelerated Markov chain Monte Carlo (MCMC) methods have been developed to reduce the sample correlation or increase effective sample size independent of the dimension (Girolami & Calderhead, 2011; Martin et al., 2012; Petra et al., 2014; Constantine et al., 2016; Cui et al., 2016; Beskos et al., 2017). Nevertheless, these random and essentially serial sampling methods

remain prohibitive for large-scale inference problems with expensive likelihoods. Deterministic methods using sparse quadratures (Schwab & Stuart, 2012; Schillings & Schwab, 2013; Chen & Schwab, 2015; 2016) were shown to converge rapidly with dimension-independent rates for problems with smooth and sparse posteriors. However, for posteriors lacking smoothness or sparsity, the convergence deteriorates significantly, despite incorporation of Hessian-based transformations (Schillings & Schwab, 2016; Chen et al., 2017).

Transport-based variational inference is another type of deterministic method that seeks a transport map in a function space (represented by, e.g., polynomials, kernels, or neural networks) that pushes the prior to the posterior by minimizing the difference between the transported prior and the posterior, measured in, e.g., Kullback–Leibler divergence (Marzouk et al., 2016; Liu & Wang, 2016; Blei et al., 2017; Bigoni et al., 2019; Detommaso et al., 2019). In particular, kernel-based Stein variational methods, using gradient-based (SVGD) (Liu & Wang, 2016; Chen et al., 2018; Liu & Zhu, 2018) and Hessian-based (SVN) (Detommaso et al., 2018; Wang & Li, 2020) optimization methods, are shown to achieve fast convergence in relatively low dimensions. Nonetheless, the convergence and accuracy of these methods deteriorates in high dimensions due to the curse of dimensionality in kernel representation. This can be partially addressed by a localized SVGD on Markov blankets, which relies on a conditional independence structure of the target distribution (Zhuo et al., 2018; Wang et al., 2018), or by a projected SVN that projects the parameter in a low-dimensional subspace (Chen et al., 2019b).

Contributions: Here, we propose, analyze, and apply a projected SVGD method to tackle the curse of dimensionality for high-dimensional nonlinear Bayesian inference problems, which relies on the fundamental property that data typically only inform a low-dimensional subspace of high-dimensional parameters, e.g., (Bashir et al., 2008; Bui-Thanh & Ghattas, 2012; Bui-Thanh et al., 2013; Spantini et al., 2015; Isaac et al., 2015; Cui et al., 2016; Chen et al., 2017; 2019a; Chen & Ghattas, 2019; Bigoni et al., 2019) and references therein. Specifically, our contributions are: (1) we perform dimension reduction by projecting the parameters to a low-dimensional subspace constructed using the gradient of the log-likelihood, and push the prior samples of the projection coefficients to their posterior by pSVGD; (2)

¹Oden Institute for Computational Engineering and Sciences, The University of Texas at Austin, Austin, USA.. Correspondence to: Peng Chen <peng@oden.utexas.edu>.

we prove the equivalence of the projected transport in the coefficient space and the transport in the projected parameter space; (3) we provide an upper bound for the projection error committed in the posterior (with the likelihood approximated by an optimal profile function) in terms of the eigenvalues of a gradient information matrix; (4) we propose adaptive and parallel algorithms to efficiently approximate the optimal profile function and the gradient information matrix; and (5) we demonstrate the accuracy (compared to SVGD) and scalability of pSVGd w.r.t. the number of parameters, samples, data points, and processor cores for a high-dimensional nonlinear Bayesian inference problem.

The major differences of this work compared to pSVN (Chen et al., 2019b): (1) pSVGd uses only gradient information of the log-likelihood, which is available for many models, while pSVN requires Hessian information, which may not be available for complex models and codes in practical applications; (2) the upper bound for the projection error w.r.t. the posterior in terms of eigenvalues is much sharper than that for pSVN in terms of projection error in parameters; (3) here we theoretically prove the equivalence of the projected transport for the coefficient and the transport for the projected parameters; (4) we also investigate the convergence of pSVGd w.r.t. the number of parameters and the scalability of pSVGd w.r.t. the number of data points.

2. Preliminaries

2.1. Bayesian Inference

Let $x \in \mathbb{R}^d$ denote a random parameter of dimension $d \in \mathbb{N}$, which has a continuous prior density $p_0 : \mathbb{R}^d \rightarrow \mathbb{R}$. Let $y = \{y_i\}_{i=1}^s$ denote a set of i.i.d. observation data. Let $f(x) := \prod_{i=1}^s p(y_i|x)$ denote, up to a multiplicative constant, a continuous likelihood of y at given x . Then the posterior density of parameter x conditioned on data y , denoted as $p : \mathbb{R}^d \rightarrow \mathbb{R}$, is given by Bayes' rule as

$$p(x) = \frac{1}{Z} f(x) p_0(x), \quad (1)$$

where Z is the normalization constant defined as

$$Z = \int_{\mathbb{R}^d} f(x) p_0(x) dx, \quad (2)$$

whose computation is typically intractable, especially for a large d and f with a complex geometry in \mathbb{R}^d , e.g., multimodal, rich local behavior, etc. The central task of Bayesian inference is to draw samples of the parameter x from its posterior distribution with density p , and compute some statistical quantity of interest, e.g., the mean and variance of the parameter x or some function of x .

2.2. Stein Variational Gradient Descent (SVGd)

SVGd is one type of variational inference method that seeks an approximation of the posterior density p by a function q^* in a predefined function set \mathcal{Q} , which is realized by minimizing the Kullback–Leibler (KL) divergence that measures the difference between two densities, i.e.,

$$q^* = \arg \min_{q \in \mathcal{Q}} D_{\text{KL}}(q|p), \quad (3)$$

where $D_{\text{KL}}(q|p) = \mathbb{E}_{x \sim q}[\log(q/p)]$, i.e., the average of $\log(q/p)$ with respect to the density q , which vanishes when $q = p$. In particular, a transport based function set is considered as $\mathcal{Q} = \{T_{\#}p_0 : T \in \mathcal{T}\}$, where $T_{\#}$ is a pushforward map that pushes the prior density to a new density $q := T_{\#}p_0$ through an invertible transport map $T(\cdot) : \mathbb{R}^d \rightarrow \mathbb{R}^d$ in a space \mathcal{T} . Let T be given by

$$T(x) = x + \epsilon \phi(x), \quad (4)$$

where $\phi : \mathbb{R}^d \rightarrow \mathbb{R}^d$ is a differentiable perturbation map w.r.t. x , and $\epsilon > 0$ is small enough so that T is invertible. It is shown in (Liu & Wang, 2016) that

$$\nabla_{\epsilon} D_{\text{KL}}(T_{\#}p_0|p)|_{\epsilon=0} = -\mathbb{E}_{x \sim p_0}[\text{trace}(\mathcal{A}_p \phi(x))], \quad (5)$$

where \mathcal{A}_p is the Stein operator given by

$$\mathcal{A}_p \phi(x) = \nabla_x \log p(x) \phi(x)^T + \nabla_x \phi(x). \quad (6)$$

Moreover, by choosing the space $\mathcal{T} = (\mathcal{H}_d)^d = \mathcal{H}_d \times \cdots \times \mathcal{H}_d$, a tensor product of a reproducing kernel Hilbert space (RKHS) \mathcal{H}_d with kernel $k(\cdot, \cdot) : \mathbb{R}^d \times \mathbb{R}^d \rightarrow \mathbb{R}$, the steepest descent direction of $D_{\text{KL}}(T_{\#}p_0|p)$ w.r.t. ϕ , denoted as $\phi_{p_0, p}^*$, is explicitly given by

$$\phi_{p_0, p}^*(\cdot) = \mathbb{E}_{x \sim p_0}[\mathcal{A}_p k(x, \cdot)], \quad (7)$$

where

$$\mathcal{A}_p k(x, \cdot) = \nabla_x \log p(x) k(x, \cdot) + \nabla_x k(x, \cdot). \quad (8)$$

Following this optimization perspective, we define a sequence of transport maps T_{ℓ} for $\ell = 0, 1, \dots$, as

$$T_{\ell}(x) = x + \epsilon_{\ell} \phi_{p_{\ell}, p}^*(x), \quad (9)$$

and $p_{\ell+1} := (T_{\ell})_{\#}p_{\ell}$, the density pushed from p_{ℓ} by the pushforward map $(T_{\ell})_{\#}$. The function $\phi_{p_{\ell}, p}^*$ is the steepest descent direction of $D_{\text{KL}}(T_{\#}p_{\ell}|p)$, which is given as in (7) with p_0 replaced by p_{ℓ} . ϵ_{ℓ} is known as a learning rate that is suitably updated in each iteration. Convergence of p_{ℓ} to the posterior p as $\ell \rightarrow \infty$ is studied in (Liu, 2017). To this end, the sequence of transport maps provide a practical algorithm for approximately drawing samples from the posterior as: first draw samples x_1^0, \dots, x_N^0 from the prior p_0 , then update them subsequently as

$$x_m^{\ell+1} = x_m^{\ell} + \epsilon_{\ell} \hat{\phi}_{p_{\ell}, p}^*(x_m^{\ell}), \quad m = 1, \dots, N, \quad (10)$$

where $\hat{\phi}_{p_\ell, p}^*(x_m^\ell)$, given by

$$\frac{1}{N} \sum_{n=1}^N \nabla_{x_n^\ell} \log p(x_n^\ell) k(x_n^\ell, x_m^\ell) + \nabla_{x_m^\ell} k(x_n^\ell, x_m^\ell), \quad (11)$$

is a sample average approximation (SAA) of $\phi_{p_\ell, p}^*(x_m^\ell)$ with samples $x_1^\ell, \dots, x_N^\ell$. The first term of (11) drives the samples to regions of high posterior density and the second term acts as a repulsive force that pushes the samples away from each other to avoid collapsing to local modes of the posterior. Note that while the posterior p defined in (1) involves the intractable normalization constant Z , $\nabla_x \log p(x)$ does not, thus making the sample update by (11) computationally efficient. For the kernel k , a common choice is Gaussian as in (Liu & Wang, 2016),

$$k(x, x') = \exp\left(-\frac{\|x - x'\|_2^2}{h}\right), \quad (12)$$

where h is the bandwidth, e.g., $h = \text{med}^2 / \log(N)$ with med representing the median of sample distances.

The repulsive force term $\nabla_x k$ in (11) plays a critical role in determining the empirical distribution of the samples. However, it is known that the kernel function in general suffers from the *curse of dimensionality* (Ramdas et al., 2015; Zhuo et al., 2018; Wang et al., 2018), which makes the repulsive term useless in high dimensions and leads to samples not representative of the posterior, as observed in (Zhuo et al., 2018; Wang et al., 2018), in which the SVGD sample variance becomes very inaccurate for large d .

3. Projected SVGD

3.1. Dimension reduction by projection

Let $\psi_1, \dots, \psi_r, \psi_{r+1}, \dots, \psi_d \in \mathbb{R}^d$ denote an orthogonal basis that spans the parameter space \mathbb{R}^d , where ψ_1, \dots, ψ_r span a subspace X_r of dimension r and $\psi_{r+1}, \dots, \psi_d$ span its complement subspace X_\perp . We define a linear projector of rank r , $P_r : \mathbb{R}^d \rightarrow \mathbb{R}^d$, as

$$P_r x := \sum_{i=1}^r \psi_i \psi_i^T x = \Psi_r w, \quad \forall x \in \mathbb{R}^d, \quad (13)$$

where $\Psi_r := (\psi_1, \dots, \psi_r) \in \mathbb{R}^{d \times r}$ represents the projection matrix and $w := (w_1, \dots, w_r)^T \in \mathbb{R}^r$ is the coefficient vector with element $w_i := \psi_i^T x$ for $i = 1, \dots, r$. By this projection, we can decompose $x \in \mathbb{R}^d$ as

$$x = x^r + x^\perp, \quad (14)$$

where the projected parameter $x^r := P_r x$ and its complement $x^\perp := P_\perp x$, with $P_\perp := I_d - P_r$ and identity matrix $I_d \in \mathbb{R}^{d \times d}$. By defining $\Psi_\perp := (\psi_{r+1}, \dots, \psi_d) \in$

$\mathbb{R}^{d \times (d-r)}$, and $w_\perp := (w_{r+1}, \dots, w_d)^T \in \mathbb{R}^{d-r}$ with elements $w_i = \psi_i^T x$ for $i = r+1, \dots, d$, we have $P_\perp x = \Psi_\perp w_\perp$. For any $x \in \mathbb{R}^d$, with the coefficient vector $w \in \mathbb{R}^r$ of the projection (13), and any $v_\perp \in \mathbb{R}^{d-r}$, we can decompose the prior density as

$$p_0(\Psi_r w + \Psi_\perp v_\perp) = p_0^r(w) p_0^\perp(v_\perp | w), \quad (15)$$

where the *marginal density* $p_0^r : \mathbb{R}^d \rightarrow \mathbb{R}$ is defined as

$$p_0^r(w) = \int_{\mathbb{R}^{d-r}} p_0(\Psi_r w + \Psi_\perp v_\perp) dv_\perp, \quad (16)$$

and the *conditional density* $p_0^\perp(\cdot | w) : \mathbb{R}^{d-r} \rightarrow \mathbb{R}$ as

$$p_0^\perp(v_\perp | w) = p_0(\Psi_r w + \Psi_\perp v_\perp) / p_0^r(w). \quad (17)$$

We seek a *profile function* $g : \mathbb{R}^d \rightarrow \mathbb{R}$ such that $g(P_r x)$ is a good approximation of the likelihood function $f(x)$ for a given projector P_r . We define a particular profile function $g^* : \mathbb{R}^d \rightarrow \mathbb{R}$ as the marginalization or conditional expectation of f w.r.t. the conditional density p_0^\perp , i.e.,

$$g^*(P_r x) = \int_{\mathbb{R}^{d-r}} f(P_r x + \Psi_\perp v_\perp) p_0^\perp(v_\perp | w) dv_\perp. \quad (18)$$

The following proposition, established in (Zahm et al., 2018), shows that g^* is the optimal profile function w.r.t. the KL divergence between the posterior density p defined in (1) and the projected posterior density $p_r : \mathbb{R}^d \rightarrow \mathbb{R}$ defined as

$$p_r(x) := \frac{1}{Z_r} g(P_r x) p_0(x), \quad (19)$$

where $Z_r := \mathbb{E}_{x \sim p_0}[g(P_r x)]$.

Proposition 1. *Given any projector P_r defined in (13), let p_r and p_r^* denote the projected posterior densities defined in (19) for any given profile function g and the profile function g^* defined in (18), respectively, then we have*

$$D_{KL}(p | p_r^*) \leq D_{KL}(p | p_r), \quad (20)$$

where p is the posterior density defined in (1).

Remark 1. *Once the projector P_r is provided, g^* defined in (18) is the optimal by Proposition 1. However, practical evaluation of g^* is challenging because (1) the basis Ψ_\perp is typically not available; (2) it involves two $(d-r)$ -dimensional integrals in (16) and (18), whose evaluation may be expensive. Several approximations were introduced in (Zahm et al., 2018). We propose an efficient approximation in Section 3.5 that is most suitable for pSVGd.*

3.2. Construction of the basis

The basis ψ_1, \dots, ψ_r introduced in last section plays a critical role for the accuracy of the approximation of the posterior density p by the optimal projected posterior density p_r^* . To construct a good basis, we first make the following assumption on the prior density.

Assumption 1. The prior density satisfies $p_0 \propto \exp(-V - W)$ for the two functions $V, W : \mathbb{R}^d \rightarrow \mathbb{R}$ such that:

(1) V is twice continuously differentiable, and there exists a symmetric positive definite matrix $\Gamma \in \mathbb{R}^{d \times d}$ such that

$$z^T \nabla^2 V(x) z \geq z^T \Gamma z$$

for any $z \in \mathbb{R}^d$ at any $x \in \mathbb{R}^d$;

(2) W is bounded in \mathbb{R}^d , and there exists a constant $\gamma \geq 1$ such that the maximum difference is bounded by

$$\sup_{x \in \mathbb{R}^d} W(x) - \inf_{x \in \mathbb{R}^d} W(x) \leq \log(\gamma).$$

Remark 2. Assumption (1) implies that the function V is at least quadratically convex such that the density decays rapidly departing from the origin. Assumption (2) guarantees that $c \exp(-V(x)) \leq \rho(x) \leq C \exp(-V(x))$ for some constants $0 < c < C$. Priors satisfying the two assumptions are Gaussian or sub-Gaussian whose tails decay at least as fast as that of Gaussian. For example, a parameter $x \in \mathbb{R}^d$ with Gaussian distribution $x \sim \mathcal{N}(\bar{x}, \Sigma)$ satisfies Assumption 1 with $\Gamma = \Sigma^{-1}$ and $\gamma = 1$.

By $H \in \mathbb{R}^{d \times d}$ we denote a gradient information matrix, which is defined as the average of the outer product of the gradient of the log-likelihood w.r.t. the posterior, i.e.,

$$H = \int_{\mathbb{R}^d} (\nabla_x \log f(x)) (\nabla_x \log f(x))^T p(x) dx. \quad (21)$$

By $(\lambda_i, \psi_i)_{i=1}^r$ we denote the generalized eigenpairs of (H, Γ) , with Γ given in Assumption 1, which correspond to the r largest eigenvalues $\lambda_1 \geq \dots \geq \lambda_r$, i.e.,

$$H \psi_i = \lambda_i \Gamma \psi_i. \quad (22)$$

In particular, for the development of pSVGD, we require $\psi_i^T \psi_j = \delta_{ij}$ instead of the conventional $\psi_i^T \Gamma \psi_j = \delta_{ij}$, being $\delta_{ij} = 1$ if $i = j$ and zero otherwise. We make the following important observation: By definition of H , the eigenvalue λ_i measures the sensitivity of the data w.r.t. the parameters along direction ψ_i , i.e., the data mostly inform parameters in directions ψ_i corresponding to large eigenvalues λ_i . For small λ_i close to zero, the variation of the likelihood f in direction ψ_i is negligible.

More rigorously, the following proposition, as shown in (Zahm et al., 2018), provides an upper bound for the projection error committed in the optimally projected posterior p_r^* in terms of the eigenvalues λ_i for $r < i \leq d$.

Proposition 2. Under Assumption 1, for the projector P_r defined in (13) with the basis ψ_1, \dots, ψ_r taken as the eigenvectors of the generalized eigenvalue problem (22), for any continuously differentiable likelihood function f satisfying $\mathbb{E}_{x \sim p_0} [(\nabla_x \log f(x))^T \Gamma^{-1} \nabla_x \log f(x)] < \infty$, we have

$$D_{KL}(p | p_r^*) \leq \frac{\gamma}{2} \sum_{i=r+1}^d \lambda_i. \quad (23)$$

To distinguish different dimensions, we consider a relative projection error defined as $\mathcal{E}_r := \sum_{i=r+1}^d \lambda_i / \sum_{i=1}^d \lambda_i$.

Remark 3. Proposition 2 implies that if the eigenvalues λ_i decay rapidly, then the projected posterior p_r^* is close to the true posterior p in KL divergence for a small $r \ll d$. Moreover, as $r \rightarrow d$, $p_r^* \rightarrow p$ if $\mathcal{E}_r \rightarrow 0$, which is usually true because of the essential ill-posedness of the inference problem due to parameter correlation, i.e., the observation data cannot inform all parameter dimensions if d is large.

Remark 4. Construction of the basis by H is challenging since H involves an integration w.r.t. the posterior distribution. We propose an algorithm in Section 3.5 for an adaptive approximation of H and construction of the basis.

3.3. Bayesian inference of the coefficient

For any $x \in \mathbb{R}^d$ with decomposition (14), or equivalently

$$x = \Psi_r w + \Psi_\perp w_\perp, \quad (24)$$

by the density decomposition (15) we have

$$p_0(x) = p_0^r(w) p_0^\perp(w_\perp | w). \quad (25)$$

For this decomposition, the projected posterior for $x \in \mathbb{R}^d$ in (19) can be written for $w \in \mathbb{R}^d$ and $w_\perp \in \mathbb{R}^{d-r}$ as

$$p_r(x) = \frac{1}{Z_r} g(\Psi_r w) p_0^r(w) p_0^\perp(w_\perp | w). \quad (26)$$

We define a new function of the coefficient vector w as

$$p^r(w) := \frac{1}{Z_r} g(\Psi_r w) p_0^r(w), \quad (27)$$

which is indeed a density function of w because by definition

$$Z_r = \mathbb{E}_{x \sim p_0} [g(P_r x)] = \mathbb{E}_{w \sim p_0^r} [g(\Psi_r w)], \quad (28)$$

where in the second equality we used the property that the randomness of x in $g(P_r x)$ can be fully represented by that of w in $g(\Psi_r w)$ due to $P_r x = \Psi_r w$. Therefore, we can view p_0^r and p^r as the prior and posterior densities of w , and $g(\Psi_r w)$ as the likelihood function. Then by the density decomposition (26), or equivalently

$$p_r(x) = p^r(w) p_0^\perp(w_\perp | w), \quad (29)$$

sampling x from the projected posterior distribution with density $p_r : \mathbb{R}^d \rightarrow \mathbb{R}$ can be conceptually realized by (1) sampling w from the posterior distribution with density $p^r : \mathbb{R}^r \rightarrow \mathbb{R}$, which is to solve a problem of Bayesian inference of the coefficient vector w of dimension r , and (2) sampling w_\perp from the conditional distribution with density $p_0^\perp(\cdot | w) : \mathbb{R}^{d-r} \rightarrow \mathbb{R}$, and (3) assembling x by the decomposition (24). However, this sampling scheme remains impractical since Ψ_\perp is in general not available or very expensive to compute, especially for large d . We defer sampling w_\perp to Section 3.5 which describes a practical algorithm and focus on sampling w from the posterior p^r by projected SVGD.

3.4. Projected SVGD

To sample from the posterior distribution of the coefficient vector w with density given by Bayes' rule in (27), we employ the SVGD method presented in Section 2.2 in the coefficient space \mathbb{R}^r , with $r < d$. Specifically, we define a projected transport map $T^r : \mathbb{R}^r \rightarrow \mathbb{R}^r$ as

$$T^r(w) = w + \epsilon \phi^r(w), \quad (30)$$

with a differentiable perturbation map $\phi^r : \mathbb{R}^r \rightarrow \mathbb{R}^r$, and a small enough $\epsilon > 0$ such that T^r is invertible. Following the argument in (Liu & Wang, 2016) on the result (5) for SVGD, we obtain

$$\nabla_{\epsilon} D_{\text{KL}}(T_{\#}^r p_0^r | p^r) \big|_{\epsilon=0} = -\mathbb{E}_{w \sim p_0^r} [\text{trace}(\mathcal{A}_{p^r} \phi^r(w))], \quad (31)$$

where \mathcal{A}_{p^r} is the Stein operator given by

$$\mathcal{A}_{p^r} \phi^r(w) = \nabla_w \log p^r(w) \phi^r(w)^T + \nabla_w \phi^r(w). \quad (32)$$

To find the perturbation map ϕ^r , we consider the space $\phi^r \in (\mathcal{H}_r)^r = \mathcal{H}_r \times \cdots \times \mathcal{H}_r$, a tensor product of RKHS \mathcal{H}_r defined with kernel $k^r(\cdot, \cdot) : \mathbb{R}^r \times \mathbb{R}^r \rightarrow \mathbb{R}$. Then the steepest descent direction of $D_{\text{KL}}(T_{\#}^r p_0^r | p^r)$ w.r.t. ϕ^r , denoted as $\phi_{p_0^r, p^r}^{r,*}$, is explicitly given by

$$\phi_{p_0^r, p^r}^{r,*}(\cdot) = \mathbb{E}_{w \sim p_0^r} [\mathcal{A}_{p^r} k^r(w, \cdot)], \quad (33)$$

where

$$\mathcal{A}_{p^r} k^r(w, \cdot) = \nabla_w \log p^r(w) k^r(w, \cdot) + \nabla_w k^r(w, \cdot). \quad (34)$$

By the same optimization perspective in the first step, we can define a sequence of transport maps T_{ℓ}^r for $\ell = 0, 1, \dots$,

$$T_{\ell}^r(w) = w + \epsilon_{\ell} \phi_{p_{\ell}^r, p^r}^{r,*}(w), \quad (35)$$

and push forward the density p_{ℓ}^r as $p_{\ell+1}^r := (T_{\ell}^r)_{\#} p_{\ell}^r$. Convergence of the density p_{ℓ}^r to the posterior density p^r as $\ell \rightarrow \infty$ can be obtained by following the same argument as in (Liu, 2017). Therefore, to draw samples from the posterior p^r , we can first draw samples w_1^0, \dots, w_N^0 from the prior with density p_0^r , and subsequently update them as

$$w_m^{\ell+1} = w_m^{\ell} + \epsilon_{\ell} \hat{\phi}_{p_{\ell}^r, p^r}^{r,*}(w_m^{\ell}), \quad m = 1, \dots, N, \quad (36)$$

where $\hat{\phi}_{p_{\ell}^r, p^r}^{r,*}(w_m^{\ell})$ is a SAA of $\phi_{p_{\ell}^r, p^r}^{r,*}(w_m^{\ell})$ with samples $w_1^{\ell}, \dots, w_N^{\ell}$, i.e., $\hat{\phi}_{p_{\ell}^r, p^r}^{r,*}(w_m^{\ell})$ is given by

$$\frac{1}{N} \sum_{n=1}^N \nabla_{w_n^{\ell}} \log p^r(w_n^{\ell}) k^r(w_n^{\ell}, w_m^{\ell}) + \nabla_{w_n^{\ell}} k^r(w_n^{\ell}, w_m^{\ell}), \quad (37)$$

where practical evaluation of the gradient of the log-posterior $\nabla_{w_n^{\ell}} \log p^r(w_n^{\ell})$, with the posterior density p^r defined in (27), is presented in Section 3.5.

The kernel k^r can be specified as in (12), i.e.,

$$k^r(w, w') = \exp \left(-\frac{\|w - w'\|_2^2}{h} \right). \quad (38)$$

To account for data impact in different directions ψ_1, \dots, ψ_r informed by the eigenvalues of (22), we propose to replace $\|w - w'\|_2^2$ in (38) by $(w - w')^T (\Lambda + I) (w - w')$ with $\Lambda = \text{diag}(\lambda_1, \dots, \lambda_r)$ for the likelihood and I for the prior.

The following theorem, proved in Appendix A, establishes the connection between pSVGd in the coefficient space and SVGD in the projected parameter space.

Theorem 1. *Under the condition $p_0^r(w) = p_0(P_r x)$ for $\Psi_r w = P_r x$, with the kernel $k^r(\cdot, \cdot) : \mathbb{R}^r \times \mathbb{R}^r \rightarrow \mathbb{R}$ defined in (38) and $k(\cdot, \cdot) : \mathbb{R}^d \times \mathbb{R}^d \rightarrow \mathbb{R}$ defined in (12), at the optimal profile function g^* in (18), we have the equivalence of the projected transport map T^r for the coefficient w in the steepest direction (33) and the transport map T for the projected parameter $P_r x$ in the steepest direction (7), as*

$$T^r(w) = \Psi_r^T T(P_r x). \quad (39)$$

In particular, we have

$$\nabla_w \log p^r(w) = \Psi_r^T \nabla_x \log p_r(P_r x), \quad (40)$$

with the posteriors p^r defined in (27) and p_r defined in (19).

Remark 5. *The equivalence (39) implies that the pSVGd only updates the projected parameter $P_r x$, or the parameter x in the subspace formed by the basis ψ_1, \dots, ψ_r , while leaving the parameter in the complement subspace unchanged. We propose an adaptive scheme (Algorithm 3) that also updates the parameter in the complement subspace.*

Remark 6. *The condition $p_0^r(w) = p_0(P_r x)$ is satisfied for p_0 such that its marginal for $P_r x$, i.e., p_0^r defined in (16), is the same as the anchored density $p_0(P_r x + \Psi_{\perp} v_{\perp})$ at $v_{\perp} = 0$. Meanwhile, Gaussian priors satisfy this condition since $p_0(P_r x + \Psi_{\perp} v_{\perp}) = p_0(P_r x) p_0(\Psi_{\perp} v_{\perp})$ where both $p_0(P_r x)$ and $p_0(\Psi_{\perp} v_{\perp})$ are Gaussian densities.*

3.5. Practical algorithms

Sampling from the projected posterior $p_r^*(x)$ defined in (19) with the optimal profile function g^* defined in (18), involves, by the decomposition (27), sampling w from the posterior p^r by pSVGd and sampling w^{\perp} from the conditional distribution with density $p_0^{\perp}(w^{\perp} | w)$. The sampling is impractical because of two challenges summarized as follows:

1. The $d - r$ basis $\Psi_{\perp} = (\psi_{r+1}, \dots, \psi_d)$ for the complement subspace, used in (16) for the marginal prior density p_0^r and in (18) for the optimal profile function g^* , are generally not available or their computation by solving the generalized eigenvalue problem (22) is too expensive for large dimension d . Meanwhile, both (16) and (18) involve high-dimensional integrals.

2. The matrix H defined in (21) for the construction of the basis ψ_1, \dots, ψ_r involves integration w.r.t. the posterior distribution of the parameter x . However, drawing samples from the posterior to evaluate the integral turns out to be the central task of the Bayesian inference.

Challenge 1 can be practically addressed by using the fundamental property pointed out in Section 3.2, i.e., the variation of likelihood f in the complement subspace X_\perp is negligible, which means that the posterior distribution meaningfully differs from the prior distribution only in the subspace X_r . Therefore, to draw samples from the posterior, we only need to proceed by the abstract Algorithm 1.

Algorithm 1 An abstract sampling procedure by projection

1. Draw samples from the prior distribution, e.g.,

$$x_n^0 \sim p_0, \quad n = 1, \dots, N.$$

2. Make parameter decomposition by projection

$$x_n^0 = P_r x_n^0 + x_n^\perp, \quad n = 1, \dots, N.$$

3. Push the projected parameter $P_r x_n^0$ in the subspace X_r to the projected posterior distribution (19) as

$$P_r x_n^\ell \sim p_r(P_r \cdot) \text{ as } \ell \rightarrow \infty, \quad n = 1, \dots, N.$$

4. Assemble the samples to approximate the posterior

$$x_n^\ell = P_r x_n^\ell + x_n^\perp, \quad n = 1, \dots, N.$$

Two important factors in Algorithm 1 have to be specified to make it practically operational: (i) the projector P_r in step 2, and (ii) the transport map in step 3.

We address (ii) at first by proposing a practical pSVGD algorithm given the projector P_r with basis Ψ_r . By the fact that the likelihood f has negligible variation in the subspace X_\perp , for any sample x_n^ℓ , $n = 1, \dots, N$, we can approximate the optimal profile function g^* in (18) as

$$g^*(P_r x_n^\ell) = f(P_r x_n^\ell + x_n^\perp), \quad (41)$$

which is equivalent to using one sample v_\perp such that $\Psi_\perp v_\perp = x_n^\perp = x_n^0 - P_r x_n^0$ to approximate the integral (18). Similarly, we can specify the projected prior density at w_n^ℓ as

$$p_0^r(w_n^\ell) = p_0(\Psi_r w_n^\ell + x_n^\perp). \quad (42)$$

By this specification, we avoid computing not only Ψ_\perp but also the high-dimensional integral w.r.t. v_\perp in both (16) and (18), thus addressing challenge 1. Moreover, under this specification, the gradient of the log-posterior $\nabla_{w_n^\ell} \log p^r(w_n^\ell)$

in (37) for the pSVGD method can be evaluated as

$$\nabla_{w_n^\ell} \log p^r(w_n^\ell) = \Psi_r^T \nabla_x \log p(\Psi_r w_n^\ell + x_n^\perp). \quad (43)$$

Given the projector P_r with basis Ψ_r , we summarize the pSVGD transport of samples in Algorithm 2.

In particular, by leveraging the property that the samples can be updated in parallel, we implement a parallel version of pSVGD using MPI for information communication in K processor cores, each with N different samples, thus producing NK different samples in total.

Algorithm 2 pSVGD in parallel

1. **Input:** samples $\{x_n^0\}_{n=1}^N$ in each of K cores, basis Ψ_r , maximum iteration L_{\max} , tolerance w_{tol} for step norm.
 2. **Output:** posterior samples $\{x_n^*\}_{n=1}^N$ in each core.
 3. Set $\ell = 0$, project $w_n^0 = \Psi_r^T x_n^0$, $x_n^\perp = x_n^0 - \Psi_r w_n^0$, and perform MPI.Allgather for coefficients $\{w_n^0\}_{n=1}^N$.
 4. **repeat**
 - 5: Compute gradients $\nabla_{w_n^\ell} \log p^r(w_n^\ell)$ by (43) for $n = 1, \dots, N$, and perform MPI.Allgather for them.
 - 6: Compute the kernel values $k^r(w_n^\ell, w_m^\ell)$ and their gradients $\nabla_{w_n^\ell} k^r(w_n^\ell, w_m^\ell)$ for $n = 1, \dots, NK$, $m = 1, \dots, N$, and perform MPI.Allgather for them.
 - 7: Update samples $w_m^{\ell+1}$ from w_m^ℓ by (36) and (37) for $m = 1, \dots, N$, with NK samples used for SAA in (37), and perform MPI.Allgather for $\{w_m^0\}_{m=1}^N$.
 - 8: Set $\ell \leftarrow \ell + 1$.
 - 9: **until** $\ell \geq L_{\max}$ or $\text{mean}(\|w_m^\ell - w_m^{\ell-1}\|_2) \leq w_{\text{tol}}$.
 - 10: Reconstruct samples $x_n^* = \Psi_r w_n^\ell + x_n^\perp$.
-

To construct the projector P_r with basis Ψ_r , we approximate H in (21) by SAA with posterior samples x_1, \dots, x_M , i.e.,

$$\hat{H} := \frac{1}{M} \sum_{m=1}^M \nabla_x \log f(x_m) (\nabla_x \log f(x_m))^T. \quad (44)$$

Since the posterior samples x_1, \dots, x_M are not available, we propose to adaptively construct the basis Ψ_r^ℓ with samples $x_1^\ell, \dots, x_M^\ell$ transported from the prior samples x_1^0, \dots, x_M^0 by pSVGD, which addresses challenge 2. This procedure is summarized in Algorithm 3. We remark that by the adaptive construction, we push the samples to their posterior in each subspace X_r^ℓ spanned by (possibly) different basis Ψ_r^ℓ with different r for different ℓ . With $\cup_\ell X_r^\ell$ exploiting all the data-informed dimensions as $\ell \rightarrow \infty$, the samples may represent the true posterior without committing projection error as bounded in Proposition 2.

4. Numerical Experiments

We present a nonlinear Bayesian inference problem with high-dimensional parameters to demonstrate the accuracy of pSVGD compared to SVGD, and the convergence and

Algorithm 3 Adaptive pSVGD in parallel

- 1: **Input:** samples $\{x_n^0\}_{n=1}^N$ in each of K cores, maximum iterations L_{\max}^x, L_{\max}^w , tolerances $x_{\text{tol}}, w_{\text{tol}}$.
- 2: **Output:** posterior samples $\{x_n^*\}_{n=1}^N$ in each core.
- 3: Set $\ell_x = 0$.
- 4: **repeat**
- 5: Compute $\nabla_x \log f(x_n^{\ell_x})$ in (44) for $n = 1, \dots, N$ in each core, and perform MPI_Allgather for them.
- 6: Solve (22) with H approximated as in (44), with all $M = NK$ samples, to get the projection basis $\Psi_r^{\ell_x}$.
- 7: Apply the pSVGD Algorithm 2, i.e.,

$$\{x_n^*\}_{n=1}^N = \text{pSVGD}(\{x_n^{\ell_x}\}_{n=1}^N, \Psi_r^{\ell_x}, L_{\max}^w, w_{\text{tol}}).$$

- 8: Set $\ell_x \leftarrow \ell_x + 1$ and $x_n^{\ell_x} = x_n^*$, $n = 1, \dots, N$.
- 9: **until** $\ell_x \geq L_{\max}^x$ or $\text{mean}(\|x_m^{\ell_x} - x_m^{\ell_x-1}\|_X) \leq x_{\text{tol}}$.

scalability of pSVGD w.r.t. the number of parameters, samples, data points, and processor cores. A linear inference example, whose posterior is analytically given, is presented in Appendix B to demonstrate the accuracy of pSVGD compared to SVGD. The code is available at <https://github.com/cpempire/pSVGD>.

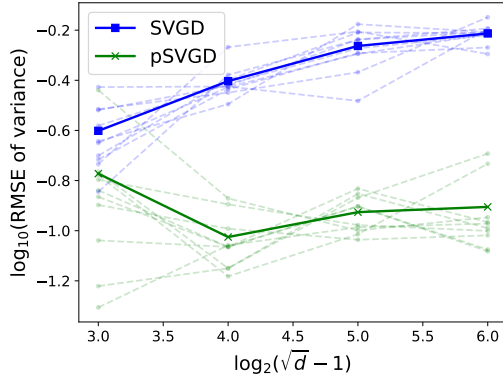


Figure 1. RMSE of pointwise sample variance in L_2 -norm, with 256 samples, SVGD and pSVGD both terminated at $\ell = 200$ iterations, parameter dimension $d = (2^n + 1)^2$, with $n = 3, 4, 5, 6$.

We consider a parameter-to-observable map $h : \mathbb{R}^d \rightarrow \mathbb{R}^s$

$$h(x) = O \circ S(x), \quad (45)$$

where $S : x \rightarrow u$ is a nonlinear discrete solution map of the log-normal diffusion model in a unit square domain

$$-\nabla \cdot (e^x \nabla u) = 0, \quad \text{in } (0, 1)^2, \quad (46)$$

imposed with Dirichlet boundary condition $u = 1$ on the top boundary and $u = 0$ on bottom boundary, and homogeneous Neumann boundary condition on the left and right boundaries. $\nabla \cdot$ is a divergence operator, and ∇ is a gradient operator. x and u are discretized by finite elements with

piecewise linear elements in a uniform mesh of triangles of size d . $x \in \mathbb{R}^d$ and $u \in \mathbb{R}^d$ are the nodal values of x and u . We consider a Gaussian distribution for $x \in \mathcal{N}(0, \mathcal{C})$ with covariance $\mathcal{C} = (-0.1\Delta + I)^{-2}$, which leads to a Gaussian distribution for $x \sim \mathcal{N}(0, \Sigma_x)$, where $\Sigma_x \in \mathbb{R}^{d \times d}$ is discretized from \mathcal{C} . $O : \mathbb{R}^d \rightarrow \mathbb{R}^s$ is a pointwise observation map at $s = 7 \times 7$ points equally distributed in $(0, 1)^2$. We consider an additive 5% Gaussian noise $\xi \sim \mathcal{N}(0, \Sigma_\xi)$ with $\Sigma_\xi = \sigma^2 I$ and $\sigma = \max(|Ou|)/20$ for data

$$y = h(x) + \xi, \quad (47)$$

which leads to the likelihood function

$$f(x) = \exp\left(-\frac{1}{2}\|y - h(x)\|_{\Sigma_\xi^{-1}}^2\right). \quad (48)$$

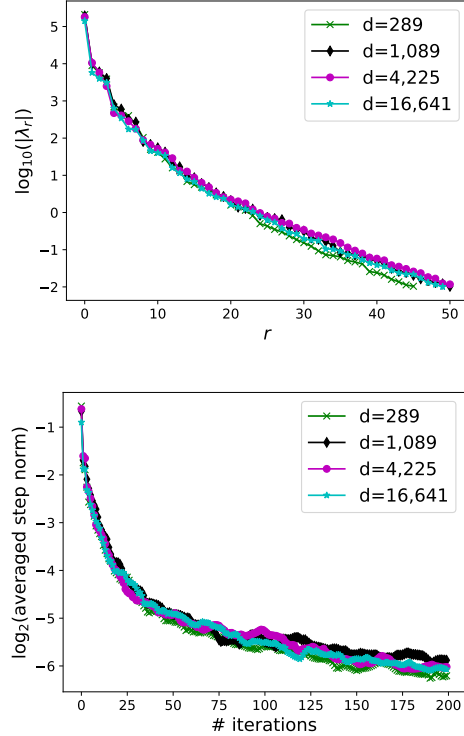


Figure 2. Scalability w.r.t. the parameter dimension d by decay of eigenvalues λ_r w.r.t. r (top), and decay of the averaged step norm $\text{mean}_m \|w_m^{\ell+1} - w_m^\ell\|_2$ w.r.t. the number of iterations (bottom).

We use a DILI-MCMC algorithm (Cui et al., 2016) to generate 10,000 effective posterior samples and use them to compute a reference sample variance. We run SVGD and the adaptive pSVGD (with $\lambda_{r+1} < 10^{-2}$) using 256 samples and 200 iterations for different dimensions, both using line search to seek the step size ϵ_ℓ . The comparison of accuracy can be observed in Figure 1. We can see that SVGD samples fail to capture the posterior distribution in high dimensions and become worse with increasing dimension,

while pSVGD samples represent the posterior distribution well, measured by sample variance, and the approximation remains accurate with increasing dimension.

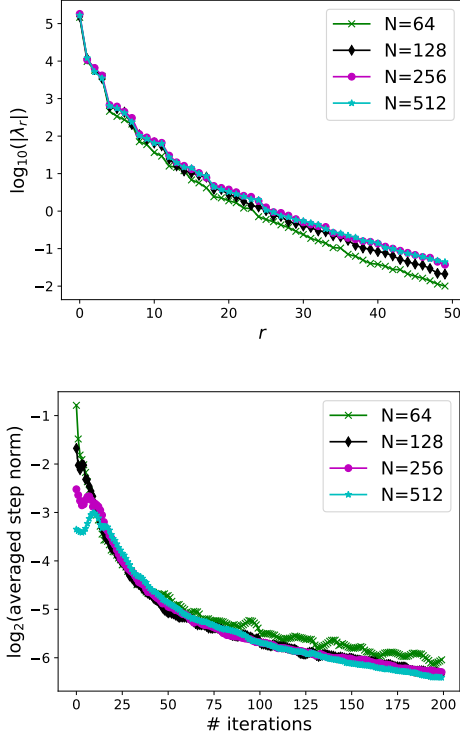


Figure 3. Scalability w.r.t. the number of samples N by decay of eigenvalues λ_r w.r.t. r (top), and decay of the averaged step norm $\text{mean}_m \|w_m^{\ell+1} - w_m^\ell\|_2$ w.r.t. the number of iterations (bottom).

The accuracy of pSVGD can be further demonstrated by the significant decay (about 7 orders of magnitude) of the eigenvalues for different dimensions in the top of Figure 2. Only about 50 dimensions (with small relative projection error, about $\mathcal{E}_r < 10^{-6}$, committed in the posterior by Proposition 2) are preserved out of from 289 to 16,641 dimensions, representing over $300\times$ dimension reduction for the last case. The similar decays of the eigenvalues λ_r in the projection rank r and the averaged step norm $\text{mean}_m \|w_m^{\ell+1} - w_m^\ell\|_2$ in the number of iterations shown in Figure 2 imply that pSVGD is scalable w.r.t. the parameter dimension. Moreover, the similar decays for different sample size $N = 64, 128, 256, 512$ in Figure 3 demonstrate that pSVGD is scalable w.r.t. the number of samples N . Furthermore, as displayed in the top of Figure 4, with increasing number of i.i.d. observation data points $s = 7^2, 15^2, 31^2, 63^2$ in a refined mesh of size $d = 17^2, 33^2, 65^2, 129^2$, the eigenvalues decay at almost the same rate with similar relative projection error \mathcal{E}_r , and lead to similar reduction d/r for r such that $\lambda_{r+1} < 10^{-2}$, which implies weak scalability of pSVGD w.r.t. the number of data points. Lastly, from the bottom of Figure 4 by the

nearly $O(K^{-1})$ decay of CPU time we can see that pSVGD achieves strong parallel scalability (in computing gradient, kernel, and sample update) w.r.t. the number of processor cores K for the same work with $KN = 1024$ samples.

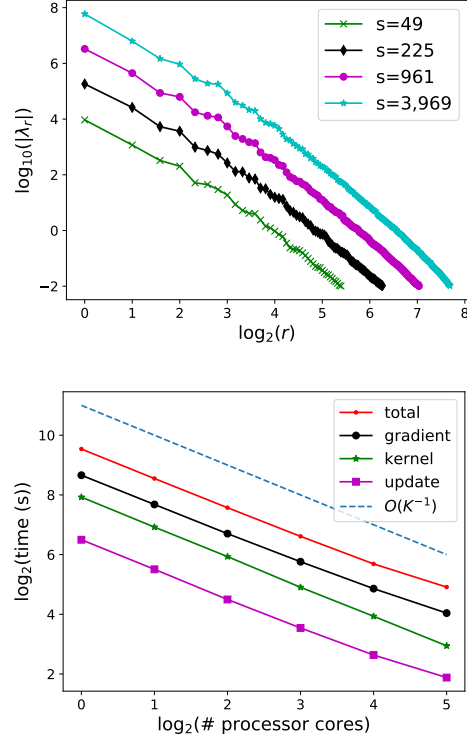


Figure 4. Scalability w.r.t. the number of data points s by decay of eigenvalues λ_r w.r.t. r (top), and the number of processor cores K by decay of CPU time for different parts of pSVGD (bottom).

5. Conclusions and Future Work

We proposed, analyzed, and demonstrated pSVGD for Bayesian inference in high dimensions to tackle the critical challenge of curse of dimensionality. The projection can be adaptively constructed by using only the information of the gradient of the log-likelihood, which is available in SVGD algorithm, where the projection error committed in the posterior can be bounded by the truncated eigenvalues. We proved that pSVGD for the coefficient is equivalent to SVGD for the projected parameter under suitable assumptions. The accuracy (compared to SVGD), convergence, and scalability of pSVGD w.r.t. the number of parameters, samples, data points, and processor cores were demonstrated by a high-dimensional nonlinear Bayesian inference problem.

Further analysis of the adaptive pSVGD and its application to other high-dimensional inference problems, e.g., Bayesian neural networks, is of interest. Another promising direction is to study the correlation, reduction by projection, and scalability in data dimension for big data applications.

References

- Bashir, O., Willcox, K., Ghattas, O., van Bloemen Waanders, B., and Hill, J. Hessian-based model reduction for large-scale systems with initial condition inputs. *International Journal for Numerical Methods in Engineering*, 73:844–868, 2008.
- Beskos, A., Girolami, M., Lan, S., Farrell, P. E., and Stuart, A. M. Geometric MCMC for infinite-dimensional inverse problems. *Journal of Computational Physics*, 335:327–351, 2017.
- Bigoni, D., Zahm, O., Spantini, A., and Marzouk, Y. Greedy inference with layers of lazy maps. *arXiv preprint arXiv:1906.00031*, 2019.
- Blei, D. M., Kucukelbir, A., and McAuliffe, J. D. Variational inference: A review for statisticians. *Journal of the American Statistical Association*, 112(518):859–877, 2017.
- Bui-Thanh, T. and Ghattas, O. Analysis of the Hessian for inverse scattering problems: I. Inverse shape scattering of acoustic waves. *Inverse Problems*, 28(5):055001, 2012.
- Bui-Thanh, T., Ghattas, O., Martin, J., and Stadler, G. A computational framework for infinite-dimensional bayesian inverse problems part I: The linearized case, with application to global seismic inversion. *SIAM Journal on Scientific Computing*, 35(6):A2494–A2523, 2013.
- Chen, P. and Ghattas, O. Hessian-based sampling for high-dimensional model reduction. *International Journal for Uncertainty Quantification*, 9(2), 2019.
- Chen, P. and Schwab, C. Sparse-grid, reduced-basis Bayesian inversion. *Computer Methods in Applied Mechanics and Engineering*, 297:84–115, 2015.
- Chen, P. and Schwab, C. Sparse-grid, reduced-basis Bayesian inversion: Nonaffine-parametric nonlinear equations. *Journal of Computational Physics*, 316:470–503, 2016.
- Chen, P., Villa, U., and Ghattas, O. Hessian-based adaptive sparse quadrature for infinite-dimensional Bayesian inverse problems. *Computer Methods in Applied Mechanics and Engineering*, 327:147–172, 2017.
- Chen, P., Villa, U., and Ghattas, O. Taylor approximation and variance reduction for PDE-constrained optimal control problems under uncertainty. *Journal of Computational Physics*, 2019a. To appear.
- Chen, P., Wu, K., Chen, J., O’Leary-Roseberry, T., and Ghattas, O. Projected Stein variational Newton: A fast and scalable Bayesian inference method in high dimensions. In *Advances in Neural Information Processing Systems*, pp. 15104–15113, 2019b.
- Chen, W. Y., Mackey, L., Gorham, J., Briol, F.-X., and Oates, C. J. Stein points. *arXiv preprint arXiv:1803.10161*, 2018.
- Constantine, P. G., Kent, C., and Bui-Thanh, T. Accelerating Markov chain Monte Carlo with active subspaces. *SIAM Journal on Scientific Computing*, 38(5):A2779–A2805, 2016.
- Cui, T., Law, K. J., and Marzouk, Y. M. Dimension-independent likelihood-informed MCMC. *Journal of Computational Physics*, 304:109–137, 2016.
- Detommaso, G., Cui, T., Marzouk, Y., Spantini, A., and Scheichl, R. A stein variational Newton method. In *Advances in Neural Information Processing Systems*, pp. 9187–9197, 2018.
- Detommaso, G., Kruse, J., Ardizzone, L., Rother, C., Köthe, U., and Scheichl, R. HINT: Hierarchical invertible neural transport for general and sequential Bayesian inference. *arXiv preprint arXiv:1905.10687*, 2019.
- Girolami, M. and Calderhead, B. Riemann manifold Langevin and Hamiltonian Monte Carlo methods. *Journal of the Royal Statistical Society: Series B (Statistical Methodology)*, 73(2):123–214, 2011.
- Isaac, T., Petra, N., Stadler, G., and Ghattas, O. Scalable and efficient algorithms for the propagation of uncertainty from data through inference to prediction for large-scale problems, with application to flow of the Antarctic ice sheet. *Journal of Computational Physics*, 296:348–368, September 2015. doi: 10.1016/j.jcp.2015.04.047.
- Liu, C. and Zhu, J. Riemannian Stein variational gradient descent for Bayesian inference. In *Thirty-Second AAAI Conference on Artificial Intelligence*, 2018.
- Liu, Q. Stein variational gradient descent as gradient flow. In *Advances in neural information processing systems*, pp. 3115–3123, 2017.
- Liu, Q. and Wang, D. Stein variational gradient descent: A general purpose Bayesian inference algorithm. In *Advances In Neural Information Processing Systems*, pp. 2378–2386, 2016.
- Martin, J., Wilcox, L., Burstedde, C., and Ghattas, O. A stochastic Newton MCMC method for large-scale statistical inverse problems with application to seismic inversion. *SIAM Journal on Scientific Computing*, 34(3): A1460–A1487, 2012.
- Marzouk, Y., Moselhy, T., Parno, M., and Spantini, A. Sampling via measure transport: An introduction. In *Handbook of Uncertainty Quantification*, pp. 1–41. Springer, 2016.

- Petra, N., Martin, J., Stadler, G., and Ghattas, O. A computational framework for infinite-dimensional Bayesian inverse problems, part ii: Stochastic Newton MCMC with application to ice sheet flow inverse problems. *SIAM Journal on Scientific Computing*, 36(4):A1525–A1555, 2014.
- Ramdas, A., Reddi, S. J., Póczos, B., Singh, A., and Wasserman, L. On the decreasing power of kernel and distance based nonparametric hypothesis tests in high dimensions. In *Twenty-Ninth AAAI Conference on Artificial Intelligence*, 2015.
- Schillings, C. and Schwab, C. Sparse, adaptive Smolyak quadratures for Bayesian inverse problems. *Inverse Problems*, 29(6):065011, 2013.
- Schillings, C. and Schwab, C. Scaling limits in computational Bayesian inversion. *ESAIM: Mathematical Modelling and Numerical Analysis*, 50(6):1825–1856, 2016.
- Schwab, C. and Stuart, A. Sparse deterministic approximation of Bayesian inverse problems. *Inverse Problems*, 28(4):045003, 2012.
- Spantini, A., Solonen, A., Cui, T., Martin, J., Tenorio, L., and Marzouk, Y. Optimal low-rank approximations of Bayesian linear inverse problems. *SIAM Journal on Scientific Computing*, 37(6):A2451–A2487, 2015.
- Wang, D., Zeng, Z., and Liu, Q. Stein variational message passing for continuous graphical models. In *International Conference on Machine Learning*, pp. 5206–5214, 2018.
- Wang, Y. and Li, W. Information Newton’s flow: second-order optimization method in probability space. *arXiv preprint arXiv:2001.04341*, 2020.
- Zahm, O., Cui, T., Law, K., Spantini, A., and Marzouk, Y. Certified dimension reduction in nonlinear Bayesian inverse problems. *arXiv preprint arXiv:1807.03712*, 2018.
- Zhuo, J., Liu, C., Shi, J., Zhu, J., Chen, N., and Zhang, B. Message passing Stein variational gradient descent. In *International Conference on Machine Learning*, pp. 6018–6027, 2018.

A. Proof of Theorem 1

Proof. We prove the equivalence at the first step $\ell = 0$. Then the equivalence for steps $\ell > 0$ follows by induction. By the parameter decomposition $x = x^r + x^\perp$ in (14) with $x^r = P_r x$, we denote π_0 and π as the prior and posterior for the projected parameter x^r , given by

$$\pi_0(x_r) = p_0(P_r x) \text{ and } \pi(x_r) = p_r(P_r x), \quad (49)$$

where p_r is the projected posterior defined in (19) with optimal profile function $g = g^*$ given in (18). Equivalently, by the property of the projection $P_r P_r x = P_r x$, we have

$$\pi(x^r) = \frac{1}{Z_r} g^*(x^r) \pi_0(x^r). \quad (50)$$

We can write the transport map (4) for the projected parameter x^r in the steepest direction $\varphi_{\pi_0, \pi}^*$ as

$$T(x^r) = x^r + \epsilon \varphi_{\pi_0, \pi}^*(x_r), \quad (51)$$

where $\varphi_{\pi_0, \pi}^*$ is given by

$$\varphi_{\pi_0, \pi}^*(\cdot) = \mathbb{E}_{x^r \sim \pi_0} [\mathcal{A}_\pi \kappa(x^r, \cdot)], \quad (52)$$

with the kernel $\kappa(x^r, \tilde{x}^r) = k(P_r x, P_r \tilde{x})$ for any $x, \tilde{x} \in \mathbb{R}^d$ and the Stein operator

$$\mathcal{A}_\pi \kappa(x^r, \cdot) = \nabla_{x^r} \log \pi(x^r) \kappa(x^r, \cdot) + \nabla_{x^r} \kappa(x^r, \cdot). \quad (53)$$

By definition of the kernel in (12), we have

$$\begin{aligned} k(P_r x, P_r \tilde{x}) &= \exp \left(-\frac{1}{h} (P_r x - P_r \tilde{x})^T (P_r x - P_r \tilde{x}) \right) \\ &= \exp \left(-\frac{1}{h} (w - \tilde{w})^T \Psi_r^T \Psi_r (w - \tilde{w}) \right) \\ &= \exp \left(-\frac{1}{h} \|w - \tilde{w}\|_2^2 \right) \end{aligned} \quad (54)$$

where we used the relation $P_r x = \Psi_r w$ and $P_r \tilde{x} = \Psi_r \tilde{w}$ in the second equality and the orthonormality $\Psi_r^T \Psi_r = I$ in the generalized eigenvalue problem (22) in the third. Therefore, by definition (38), we have

$$k^r(w, \tilde{w}) = \kappa(x^r, \tilde{x}^r). \quad (55)$$

Moreover, for the gradient of the kernel we have

$$\begin{aligned} \nabla_{x^r} \kappa(x^r, \tilde{x}^r) &= -\frac{2}{h} \kappa(x^r, \tilde{x}^r) (x^r - \tilde{x}^r) \\ &= -\frac{2}{h} \kappa(x^r, \tilde{x}^r) \Psi_r (w - \tilde{w}). \end{aligned} \quad (56)$$

On the other hand, we have

$$\nabla_w k^r(w, \tilde{w}) = -\frac{2}{h} k^r(w, \tilde{w}) (w - \tilde{w}), \quad (57)$$

which yields

$$\nabla_w k^r(w, \tilde{w}) = \Psi_r^T \nabla_{x^r} \kappa(x^r, \tilde{x}^r). \quad (58)$$

For the posterior π defined in (49), we have

$$\nabla_{x^r} \log \pi(x^r) = \frac{\nabla_{x^r} (g^*(x^r) \pi_0(x^r))}{g^*(x^r) \pi_0(x^r)}, \quad (59)$$

while for the posterior p^r defined in (27), we have

$$\nabla_w \log p^r(w) = \frac{\nabla_w (g^*(\Psi_r w) p_0^r(w))}{g^*(\Psi_r w) p_0^r(w)}. \quad (60)$$

By chain rule, it is straightforward to see that

$$\nabla_w g^*(\Psi_r w) = \Psi_r^T \nabla_{x^r} g^*(x^r). \quad (61)$$

Under assumption $p_0^r(w) = p_0(P_r x)$ in Theorem 1, and $p_0(P_r x) = \pi_0(x^r)$ by definition (49), we have

$$\nabla_w p_0^r(w) = \Psi_r^T \nabla_{x^r} \pi_0(x^r). \quad (62)$$

Therefore, combining (61) and (62), we have

$$\nabla_w \log p^r(w) = \Psi_r^T \nabla_{x^r} \log \pi(x^r). \quad (63)$$

To this end, we obtain the equivalence of the Stein operators

$$\mathcal{A}_{p^r} k^r(w, \tilde{w}) = \Psi_r^T \mathcal{A}_\pi \kappa(x^r, \tilde{x}^r) \quad (64)$$

for $x^r = \Psi_r w$ and $\tilde{x}^r = \Psi_r \tilde{w}$. Since the prior densities $\pi_0(x^r) = p_0^r(w)$, we have the equivalence

$$\mathbb{E}_{w \sim p_0^r} [\mathcal{A}_{p^r} k^r(w, \tilde{w})] = \Psi_r^T \mathbb{E}_{x^r \sim \pi_0} [\mathcal{A}_\pi \kappa(x^r, \tilde{x}^r)], \quad (65)$$

which concludes the equivalence of the transport map (39) by $w = \Psi_r^T x^r$ with the same ϵ at $\ell = 0$. Moreover, by induction we have

$$T_\ell^r(w^\ell) = \Psi_r^T T_\ell(P_r x^\ell), \quad (66)$$

which concludes. \square

B. A linear inference problem

We consider a linear parameter-to-observable map $A : \mathbb{R}^d \rightarrow \mathbb{R}^s$, which is given by

$$Ax = O \circ Bx, \quad (67)$$

where $B : x \rightarrow u$ is a linear discrete solution map of the diffusion reaction equation (Δ is the Laplace operator)

$$-\Delta u + u = x, \quad \text{in } (0, 1), \quad (68)$$

with boundary condition $u(0) = 0$ and $u(1) = 1$, which is solved by a finite element method. The continuous parameter x and solution u are discretized by finite elements

with piecewise linear elements in a uniform mesh of size d . $x \in \mathbb{R}^d$ and $u \in \mathbb{R}^d$ are the nodal values of x and u . The parameter x is assumed to follow a Gaussian distribution $\mathcal{N}(0, \mathcal{C})$ with covariance $\mathcal{C} = (-0.1\Delta + I)^{-1}$, which leads to a Gaussian parameter $x \sim \mathcal{N}(0, \Sigma_x)$, with covariance $\Sigma_x \in \mathbb{R}^{d \times d}$ as a discretization of \mathcal{C} .

$O : \mathbb{R}^d \rightarrow \mathbb{R}^s$ in (67) is an observation map that take s components of u that are equally distributed in $(0, 1)$. For $s = 15$, we have $Ou = (u(1/16), \dots, u(15/16))^T$. We assume an additive 1% Gaussian noise $\xi \sim \mathcal{N}(0, \Sigma_\xi)$ with $\Sigma_\xi = \sigma^2 I$ and $\sigma = \max(|Ou|)/100$ for data

$$y = Ax + \xi, \quad (69)$$

then the likelihood function is given by

$$f(x) = \exp\left(-\frac{1}{2}\|y - Ax\|_{\Sigma_\xi^{-1}}^2\right). \quad (70)$$

Because of the linearity of the inference problem, the posterior of x is also Gaussian $\mathcal{N}(x_{\text{MAP}}, \Sigma_y)$ with the MAP point $x_{\text{MAP}} = \Sigma_y A^T \Sigma_\xi^{-1} y$ and covariance

$$\Sigma_y = (A^T \Sigma_\xi^{-1} A + \Sigma_x^{-1})^{-1}. \quad (71)$$

We run SVGD and pSVGd (projection with $r = 8$ basis functions and $\lambda_9 < 10^{-4}$) with 256 samples and 200 iterations for different dimensions, both using line search to seek the step size ϵ_ℓ . The RMSE (of 10 trials and their average) of the samples variances compared to the ground truth (71) are shown in Figure 5, which indicates that SVGD deteriorates with increasing dimension while pSVGd performs well for all dimensions.

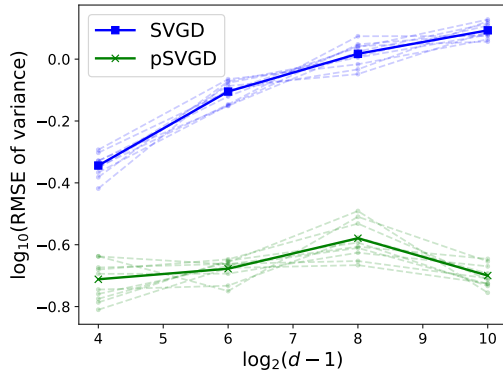


Figure 5. RMSE of pointwise sample variance in L_2 -norm, with 256 samples, SVGD and pSVGd both terminated at $\ell = 200$ iterations, parameter dimension $d = 2^n + 1$, with $n = 4, 6, 8, 10$.